Physica D 237 (2008) 3123–3134

Contents lists available at ScienceDirect

Physica D

journal homepage: www.elsevier.com/locate/physd

Dipole and quadrupole solitons in optically-induced two-dimensional defocusing photonic lattices

H. Susanto [a], K.J.H. Law [a], P.G. Kevrekidis [a,*], L. Tang [b], C. Lou [b], X. Wang [c], Z. Chen [b,c]

[a] *Department of Mathematics and Statistics, University of Massachusetts, Amherst, MA 01003, USA*

[b] *The Key Laboratory of Weak-Light Nonlinear Photonics, Ministry of Education, and TEDA Applied Physical School, Nankai University, Tianjin 300457, China*

[c] *Department of Physics and Astronomy, San Francisco State University, San Francisco, CA 94132, USA*

ARTICLE INFO

Article history:
Received 1 September 2007
Received in revised form
15 May 2008
Accepted 29 May 2008
Available online 12 June 2008
Communicated by S. Kai

PACS:
05.45.Yv
42.65.Jx
42.65.Hw
42.65.Tg

Keywords:
Dipoles
Quadrupoles
Solitons
Defocusing photonic lattices

ABSTRACT

Dipole and quadrupole solitons in a two-dimensional optically induced defocusing photonic lattice are theoretically predicted and experimentally observed. It is shown that in-phase nearest-neighbor and out-of-phase next-nearest-neighbor dipoles exist and can be stable in the intermediate intensity regime. There are also different types of dipoles that are always unstable. In-phase nearest-neighbor quadrupoles are also numerically obtained, and may also be linearly stable. Out-of-phase, nearest-neighbor quadrupoles are found to be typically unstable. These numerical results are found to be aligned with the main predictions obtained analytically in the discrete nonlinear Schrödinger model. Finally, experimental results are presented for both dipole and quadrupole structures, indicating that self-trapping of such structures in the defocusing lattice can be realized for the length of the nonlinear crystal (10 mm).

© 2008 Elsevier B.V. All rights reserved.

1. Introduction

Self-trapping of light in photonic lattices optically induced in nonlinear photorefractive crystals, such as strontium barium niobate (SBN) has attracted a considerable amount of attention, ever since its theoretical inception [1] and experimental realization [2–4]. This is perhaps, primarily because it constitutes a setting where it is very natural to consider the competing effects of nonlinearity with diffraction, and to study the effects of periodic "potentials" on solitary waves; here the role of the "potential" is played by the ordinary polarization of light forming a waveguide array in which the extra-ordinarily polarized probe beam evolves.

This setting has provided a fertile ground for the experimental realization and detailed examination of many interesting concepts of nonlinear wave physics, including, for instance, the formation of discrete dipole [5], necklace [6] solitons and even stripe patterns [7], rotary solitons [8], discrete vortices [9] or the realization of photonic quasicrystals [10] and Anderson localization [11]. It is clear from these findings that this setting can serve not only as a host for the examination of localized structures that may be usable as carriers and conduits for data transmission and processing in all-optical communication schemes; it is also relevant as an experimentally tunable playground where numerous fundamental issues of solitons and nonlinear waves can be explored.

It is interesting to mention in passing that in parallel (and nearly concurrently) to this direction of photorefractive crystal lattices, a number of other venues were developed in optical and atomic physics, where the interplay of nonlinearity with periodicity is important for the observed dynamics. Such contexts involve on the optical end, the numerous developments on the experimental and theoretical investigation of optical waveguide arrays; see e.g. [12,13] for relevant reviews. On the atomic physics end, the confinement of dilute alkali vapors in optical lattice potentials [14] has similarly offered the opportunity to examine many fundamental phenomena involving spatial periodicity, including the manifestation of modulational instabilities, Bloch oscillations, Landau–Zener tunneling and gap solitons among others; see [15] for a recent review.

In the present study, motivated by SBN crystals and photorefractive lattices, we focus on two-dimensional periodic, nonlinear media. In such settings, the vast majority of studies have centered around focusing nonlinearities; the reason for this is two-fold: on

---

[*] Corresponding author.
E-mail address: kevrekid@math.umass.edu (P.G. Kevrekidis).

0167-2789/$ – see front matter © 2008 Elsevier B.V. All rights reserved.
doi:10.1016/j.physd.2008.05.017

the theoretical end, the topic of focusing solitary waves is interesting due to the collapse (and concomitant arrest by the lattice) phenomena in the case of cubic nonlinearity [16]. On the other hand, in the photorefractive case, collapse is absent due to the saturable nature of the nonlinearity; however, in the latter case, it is technically easier to work with voltages that are in the regime of focusing rather than in that of the defocusing nonlinearity (in the latter case, sufficiently large voltage, which is tantamount to large nonlinearity, may cause damage to the crystal). Hence, the only coherent structure that appears to be explored in the defocusing regime experimentally appears to be that of fundamental gap solitons excited in the vicinity of the edge of the first Brillouin zone [2]. More complex gap structures appear not to have been studied systematically, perhaps partially due to the above reasons. In an earlier work [17], motivated by the above lack of results, we considered more complicated multipole (i.e., dipole and quadrupole)[1] and vortex structures in the defocusing case for a standard discrete dynamical lattice (namely, the discrete nonlinear Schrödinger equation with cubic nonlinearity [18]). This provided us with an analytically tractable and numerically accessible roadmap for the study of some of the relevant solutions. In the present work, we employ a continuum model involving a periodic potential and a saturable nonlinearity as associated with the SBN crystals. In particular, we demonstrate both experimentally and numerically multipole (dipoles and quadrupoles) solitons in 2D square lattices induced with a self-defocusing nonlinearity. We numerically analyze both the existence and the stability of these structures and follow their dynamics, in the cases where we find them to be unstable. We also qualitatively compare our findings with the roadmap provided by the *discrete* model [17].

Our presentation is structured as follows. In Section 2, we present our theoretical setup (related to our experiments). Dipole solutions with the two excited sites in adjacent wells of the periodic potential (nearest-neighbor dipoles) are studied in Section 3. Subsequently, we do the same for next-nearest-neighbor dipoles (excited in two diagonal sites of the square lattice) in Section 4. Section 5 addresses the case of quadrupoles, and Section 6 presents our experimental results for the structures examined. Finally, in Section 7, we summarize our findings, posing some interesting questions for future study.

2. Setup

For our theoretical considerations, we use the non-dimensionalized version of the photorefractive model with the saturable nonlinearity, as developed in detail in [19,20], in the following form:

$$\mathrm{i}U_z = -\left(U_{xx} + U_{yy}\right) - \frac{E_0}{1 + I_{ol} + |U|^2} U. \tag{1}$$

In the above expression U is the slowly varying amplitude of the probe beam normalized by $(I_d)^{1/2}$, where I_d is the dark irradiance of the crystal, and

$$I_{ol} = I_0 \cos^2\left(\frac{x+y}{\sqrt{2}}\right) \cos^2\left(\frac{x-y}{\sqrt{2}}\right), \tag{2}$$

is a square optical lattice intensity function in units of I_d. Here I_0 is the lattice peak intensity, z is the propagation distance (in units of $2k_1 D^2/\pi^2$), (x, y) are transverse distances (in units of D/π), E_0 is the applied DC field voltage (in units of $\pi^2(k_0^2 n_e^4 D^2 r_{33})^{-1}$), D is the lattice spacing, $k_0 = 2\pi/\lambda_0$ is the wavenumber of the laser in the vacuum, λ_0 is the wavelength, n_e is the refractive index for an extraordinarily polarized beam, $k_1 = k_0 n_e$, and r_{33} is the electro-optic coefficient for the extraordinary polarization. In line with our experiment, we choose the lattice intensity $I_0 = 5$ (in units of I_d). A plot of the optical lattice is shown in Fig. 1, also for illustrative purposes regarding the location where our localized pulses will be "inserted". In addition, we choose other physical parameters consistently with the experiment as

$$D = 25~\mu\text{m}, \quad \lambda_0 = 0.5~\mu\text{m}, \quad n_e = 2.3, \quad r_{33} = 280~\text{pm/V}.$$

Thus, in this paper, one x or y unit corresponds to 7.96 µm, one z unit corresponds to 3.66 mm, and one E_0 unit corresponds to 12.76 V/mm in physical units. In the experiments, the applied DC field is −110 V/mm, which gives $E_0 = 8.62$ in our numerical simulations.

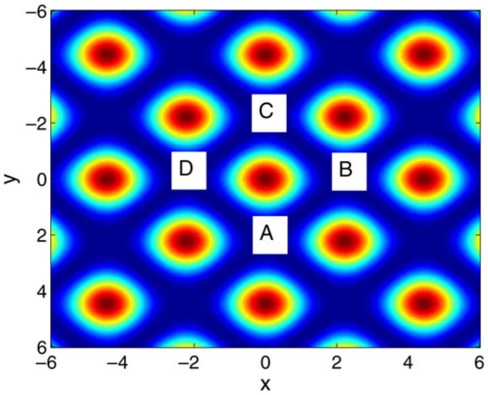

Fig. 1. (Color online) A spatial (x–y) contour plot of the ordinary polarization standing wave [lattice beam in Eq. (1)]. The localized pulses will be sitting at the minima of the lattice field, as opposed to the focusing nonlinearity lattice field, where they reside at the maxima. Points A, B, C, and D are used for naming the dipole configurations. A is a nearest-neighbor minimum of B and D (in our "diagonally-oriented" lattice), while it is a next-nearest-neighbor of C. Because of that, dipoles whose two lobes are at A and B (or at C and D) will be called nearest-neighbor dipole solitons. The ones that are sitting at A and C (or at B and D) will be called next-nearest-neighbor dipoles.

It should also be noted here that in our experimental results the diffraction length can be approximately evaluated (for the beams widths and wavelengths that we typically used) as being 2.5 mm. As our crystal extends over 10 mm in the z-direction, it is clear that the patterns that we observe are over a few (roughly 4) diffraction lengths and hence if they are self-supported within such length scales, this will indicate that they are indeed self-trapped beams. On the other hand, as we will see in what follows (in our numerical simulations), for all the configurations that we will find to be unstable, the instability development will arise typically for dimensionless propagation distances of $10 < z < 100$. Since these distances are considerably longer (in dimensional units) than the propagation distance in our crystal, all of the patterns presented in Sections 3–5 (even the most unstable ones) should, in principle, be experimentally observable in our setting. This is corroborated by our experimental results in Section 6.

The numerical simulations are done with an uniform spatial mesh with $\Delta x = 1/3$ and domain size 30×30, i.e. 91×91 grid points for most configurations (see Fig. 1 for a schematic of the spatial configurations). For some of the configurations, a larger domain was required, in which case a domain of size 60×60, i.e. 181×181 grid points, was used. Regarding the typical dynamics of a soliton when it is unstable, we simulate the z-dependent behavior using a Runge–Kutta fourth-order method using a step $\Delta z = 0.00025$.

---

[1] It should be pointed out here that although in the standard electromagnetic convention, one thinks of dipoles as bearing two opposite charges, and quadrupoles as bearing two positive and two negative charges (in our case, phases of the excited sites), here we will use a different notational convention. More specifically, following the etymology of the words, we will refer to any two-site excitation as a dipole, and to any four-site excitation as a quadrupole herein.

Stationary solutions of Eq. (1) are sought in the form of $U(x,y,z) = u(x,y)\mathrm{e}^{\mathrm{i}\mu z}$, where μ is the propagation constant and u is a real valued function satisfying

$$\mu u - \left(u_{xx} + u_{yy}\right) - \frac{E_0}{1 + I_{ol} + u^2} u = 0. \tag{3}$$

The localized states $u(x,y)$ of (3) were obtained using the Newton–Krylov fixed point solver *nsoli* from [21] and continuation was used as a function of μ, to follow the relevant branches of solutions.

The propagation constant μ we consider in this report is in the first spectral gap. Using Hill's method for the 2D problem [22], for parameter values mentioned above, we find the band gap to be $4.2 \lesssim \mu \lesssim 5.46$.[2]

The power or the norm of the solitary waves is defined as follows:

$$P = \left[\int_{-\infty}^{\infty}\int_{-\infty}^{\infty} |U|^2 \,\mathrm{d}x\mathrm{d}y\right]^{1/2}. \tag{4}$$

We analyze the linear stability of soliton solutions $u(x,y)$ of (3) by applying an infinitesimal perturbation to them. Writing $U(x,y,z) = \mathrm{e}^{\mathrm{i}\mu z}\left(u(x,y) + \mathrm{e}^{\lambda z}\tilde{u}(x,y)\right)$, the perturbation $\tilde{u}(x,y)$ will then satisfy the following linearized equation

$$\mathrm{i}\lambda\tilde{u} = \mu\tilde{u} - \left(\tilde{u}_{xx} + \tilde{u}_{yy}\right) - \frac{E_0}{\left(1 + I_{ol} + u^2\right)^2}\left[\left(1 + I_{ol}\right)\tilde{u} - u^2\tilde{u}^*\right], \tag{5}$$

where the superscript $*$ denotes complex conjugation. We solve the above linear eigenvalue problem using MATLAB's standard eigenvalue solver package.

At this point, it is also relevant to summarize the results of the *discrete* NLS defocusing model of [17] that we will use for comparison with the findings below. These results are incorporated in Table 1, where the stability of all the possible combinations of in-phase and out-of-phase, nearest-neighbor and next-nearest-neighbor configurations is quantified in terms of their relevant eigenvalues of linearization. The configurations are dubbed unstable when they possess (for all parameter values) real eigenvalue pairs, whereas they are considered marginally stable when they do not always have such pairs. However, the latter configurations typically, in this setting, possess imaginary eigenvalues with negative Krein signature (see e.g. [23] and references therein), which practically means that if these collide with other eigenvalues, as μ is varied, complex eigenvalue quartets will emerge out of Hamiltonian–Hopf bifurcations [24], destabilizing the relevant solution. Hence, such solutions are not *always* linearly unstable, but *may become* unstable for some parameter ranges.

Table 1
Summary of the stability results of the discrete model with cubic nonlinearity, studied in [17], for all the in-phase (IP) and out-of-phase (OOP), nearest-neighbor (NN), as well as next-nearest-neighbor (NNN) configurations

	NN stability	NNN stability
IP dipole	Stable ($N_i^- = 1$)	Unstable ($N_r = 1$)
OOP dipole	Unstable ($N_r = 1$)	Stable ($N_i^- = 1$)
IP quadrupole	Stable ($N_i^- = 3$)	Unstable ($N_r = 3$)
OOP quadrupole	Unstable ($N_r = 3$)	Stable ($N_i^- = 3$)

N_r denotes real eigenvalue pairs and N_i^- denotes imaginary eigenvalue pairs with negative Krein signature.

3. Nearest-neighbor dipole solitons

In this section, we report dipole solitons where the two lobes of the wave are located in two nearest-neighbor (NN) lattice sites in the 2D square lattice potential shown in Fig. 1. The lobes can have the same phase or π phase difference and are, accordingly, hereafter termed in-phase (IP) dipoles and out-of-phase (OOP) dipoles, respectively. Notice that due to the (diagonal) nature of our lattice, the nearest-neighbor configurations that we consider are "built" along the diagonal direction.

3.1. In-phase nearest-neighbor dipole solitons

We have found IP dipoles in a large interval of propagation constants μ for the given voltage E_0. We found that the solitons exist for μ smaller than 5.46, or for peak intensities larger than 0.144. We note that the intensity of the dipoles cannot be arbitrarily low, a result similar to the observed results of the focusing case [5,20]. The relevant findings are summarized in Fig. 2.

The top left panel of Fig. 2 shows the stability of the dipoles as a function of the propagation constant μ, by illustrating the maximal growth rate (maximum real part over all perturbation eigenvalues) of perturbations. When $\max(\mathrm{Re}(\lambda)) = 0$, this implies stability of the configuration, while the configuration is unstable if $\max(\mathrm{Re}(\lambda)) \neq 0$ in this Hamiltonian system. We found that the stability region of this type of dipoles is given by $4.2 \le \mu \le 4.91$, the left hand limit corresponding to the Bloch band. The top right panel depicts the peak intensity and the power of the dipoles. The middle left and right panels show the profile u of a dipole at $\mu = 5$ and the corresponding spectra at the complex plane, respectively. We see that the soliton is unstable due to an oscillatory instability. This is the typical instability in this case, in line with the discrete cubic model results. Clearly, there is an imaginary eigenvalue with negative Krein signature [23] which, upon collisions with the continuous spectrum results in Hamiltonian–Hopf bifurcations and concomitant oscillatory instabilities.

As we increase μ further, the dipoles disappear in a saddle-node bifurcation. The bifurcation diagram is depicted in the top panels of Fig. 2. At the bifurcation point, $\mathrm{d}P/\mathrm{d}\mu \to \infty$, as $\mu \to 5.46$, i.e., at the boundary of the first Bloch band. At this point, the IP NN configuration collides with a different configuration shown at the bottom panel of Fig. 2 (where the two nearest-neighbors -along the axis of the dipole- of the two populated wells are populated out-of-phase with them) and disappears in a saddle-node bifurcation. The corresponding profile and spectral plane for the saddle branch at $\mu = 5$ is shown in the bottom right panel of the same figure, illustrating the strong instability of the latter.

We have also simulated the dynamics of the solitary waves when they are unstable. In Fig. 3 we present the evolution of the unstable dipoles shown in Fig. 2. The dipoles are perturbed by a random noise with maximum intensity 0.25% of the soliton peak intensity. Shown in Fig. 3 are the isosurfaces and the slices of the soliton along the propagation direction.

The dynamics of the soliton shown in the middle panel of Fig. 2 is presented in the top panels of Fig. 3. One can see that even with

---

[2] We note that the linear spectrum for μ quoted here and shown in the following images was the most accurate we computed using Hill's method based on consistency over Δx in the limit $\Delta x \to 0$. The linear spectrum for the discretized problem with our chosen discretization is slightly different however, and in particular, the first band edge occurs at a slightly larger value of μ. It is interesting to note that, for the families of solutions investigated herein, all saddle node bifurcations were found to occur very close to the accurate band edge (in the gap), while those solutions which degenerate to linear Bloch modes actually degenerate beyond this value at the band edge particular to the discretization (not shown).

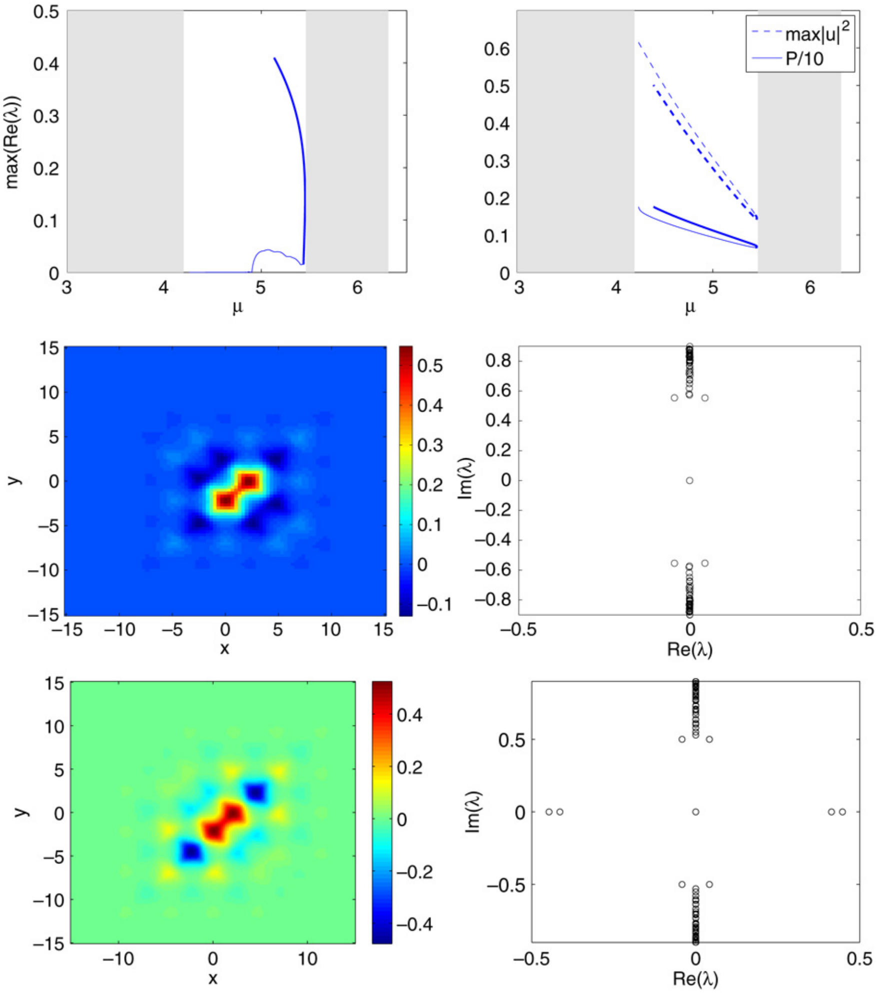

Fig. 2. (Color online) The top left panel shows the stability of the dipoles as a function of the propagation constant μ. It is stable when the spectrum is purely imaginary (i.e., when $\max(\mathrm{Re}(\lambda)) = 0$). The top right panel depicts the peak intensity and the power of the dipoles. The thin line corresponds to the solution represented in the middle row, while the bold line corresponds to the waveform illustrated in the bottom row. These two branches of solutions collide and mutually annihilate in a saddle-node bifurcation. The shaded areas in both of these panels represent the bands of the periodic potential. The middle (resp. bottom) left and right panels show the profile u of the branch indicated by thin (resp. bold) line in the top row at $\mu = 5$ and the corresponding complex spectral plane $(\mathrm{Re}(\lambda), \mathrm{Im}(\lambda))$ of the eigenvalues $\lambda = \mathrm{Re}(\lambda) + \mathrm{i}\,\mathrm{Im}(\lambda)$.

that strong perturbation, at $z = 100$ the soliton still resembles its initial configuration. Physically, this corresponds to a propagation distance of approximately 366 mm. This means that the instability is very unlikely to be observed in the photorefractive crystal lattice used in our experiments. For longer propagation distances, the oscillatory instability sets in and finally rearranges the dipole into a fundamental soliton type configuration principally centered around a single site.

For the dipole shown in the bottom panel of Fig. 2, we present its dynamics as bottom panels of Fig. 3. We found that the instability is strong as predicted above, such that even after a relatively short propagation distance, the configuration turns into the more stable solution of the IP NN dipole branch. We did not present the further dynamics of the dipole, as it is similar to the upper panels.

3.2. *Out-of-phase nearest-neighbor dipole solitons*

We have also found OOP dipoles arranged in nearest-neighboring lattice wells. We summarize our findings in Fig. 4 where one can see that the solitons exist in the whole entire region of propagation constant μ in the first Bragg gap, $\mu \in (4.2, 5.46)$. This smooth transition indicates that the OOP NN dipole solitons emerge out of the Bloch band waves; see e.g. [25,26] for a relevant discussion of the 1D and of the 2D problem respectively, in the case of the cubic nonlinearity. Nonetheless, the OOP NN dipoles are typically unstable due to a real eigenvalue pair. Notice that this is in agreement with the prediction of the discrete model (as can be seen from Table 1). As the branch merges with the band edge, we observe an interesting feature, namely that the configuration resembles that of a quadrupole with a π phase difference between two neighboring solitons, which we call $+-+-$ quadrupoles below. This can be an indication that these structures bifurcate out of the Bloch band from the same bifurcation point. We elaborate this further in our discussion of the quadrupole structures in Section 5.

In Fig. 5 we present the instability dynamics of an OOP NN dipole soliton perturbed by similar random noise perturbation as in Fig. 3. This type of dipoles is typically more unstable than its IP counterpart, as is illustrated in the figure. In particular, in this example of unstable evolution even at $z = 10$, the instability already manifests itself. One similarity of the instability of OOP NN dipoles with that of the IP NN ones is that the dipoles tend to degenerate to a single-site, fundamental gap soliton, which is stable in this setting. We note in passing that similar evolution results for dipoles and quadrupoles (but for short propagation distances) in the focusing case are discussed in [20].

Fig. 3. (Color online) The evolution of the dipoles shown in Fig. 2 perturbed by a random noise of maximum intensity 0.25% of the soliton peak intensity. Presented in the figure are the isosurfaces (left panels) of height 0.2 for the first configuration (top panels) and of height 0.1 for the second one (bottom panels) and their slices at some instances (right panels).

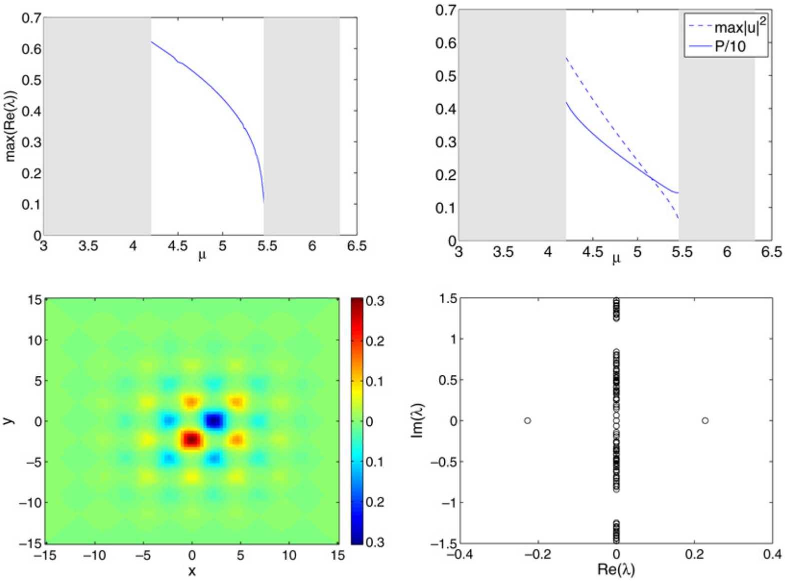

Fig. 4. (Color online) The top panels correspond to the same panels of Fig. 2 but for OOP NN dipole solitons. The bottom panel show the profile u and the corresponding spectrum in the complex plane of the dipoles at $\mu = 5.4$.

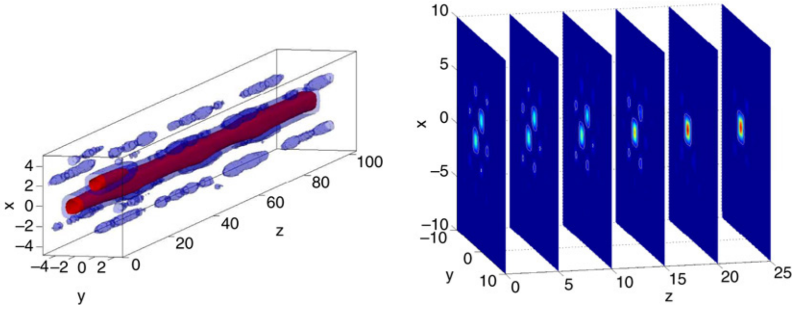

Fig. 5. (Color online) Similar to Fig. 3 but for the evolution of OOP NN dipoles. Shown are the isosurfaces of height 0.05 (red) and 0.015 (blue) and the contour plot slices at some select propagation distances.